ACADÉMIE
DES SCIENCES
INSTITUT DE FRANCE

Comptes Rendus
Mécanique

Atika Kabouya and Ali Belhamra

Hydrodynamic lubrication study of plain journal bearings lubricated with couple stress fluids: surface texture effects

Volume 354 (2026), p. 71-87

Online since: 5 February 2026

https://doi.org/10.5802/crmeca.347

The Comptes Rendus. Mécanique *are a member of the Mersenne Center for open scientific publishing*
www.centre-mersenne.org — e-ISSN : 1873-7234

ACADÉMIE DES SCIENCES
INSTITUT DE FRANCE

Comptes Rendus. Mécanique
2026, Vol. 354, p. 71-87
https://doi.org/10.5802/crmeca.347

Research article

Hydrodynamic lubrication study of plain journal bearings lubricated with couple stress fluids: surface texture effects

Atika Kabouya [*, a] **and Ali Belhamra** [a]

[a] Electro Mechanics Department, Electromechanical Systems Laboratory, Faculty of Technology, University Badji Mokhtar, 12, PO Box, Annaba, 23000, Algeria

E-mails: atika.kabouya@univ-annaba.dz (A. Kabouya), belhamraali@yahoo.fr (A. Belhamra)

Abstract. This study investigates the static characteristic of textured bearings lubricated with oils containing viscosity additives, thus influencing their tribological performance. The texture model adopted is that of the positive sinusoidal half-wave, a configuration that enables lubrication to be optimized by modifying the distribution of the fluid film. The lubricant used has a non-Newtonian rheological behavior, and is modeled as a couple stress fluids, taking into account the effects of fluid microstructure on flow.

The results obtained are analyzed by comparing them with those of a plain bearing lubricated by a conventional Newtonian fluid, enabling the influence of the lubricant's texturing and properties on bearing performance to be assessed. It is shown that the combination of the surface texturing of the pad and lubrication with polar fluids has significant effects on the static characteristics of the journal bearing, such as: load-carrying capacity, friction factor, attitude angle, and side leakage flow. It is also found that the sensitivity of these effects increases with the couple stress parameter and the eccentricity ratio.

Keywords. Hydrodynamic lubrication, Hydrodynamic bearing, Couple stress fluid, Non-Newtonian fluid, Surface texture.

Manuscript received 15 March 2025, revised 24 July 2025 and 16 October 2025, accepted 20 January 2026, online since 5 February 2026.

1. Introduction

The current trend in modern engineering is to reduce weight and operate at supersonic speeds. These conditions have an effect on the characteristics of journal bearings, and may lead to exceeding the safety limits of these components. For precise prediction of bearing performance, it is necessary to develop numerical simulations that consider the impact of parameters neglected by Reynolds [1] in classical lubrication theory, such as the surface state and the rheology of lubricant. So, the development of micro texturing processes [2,3], the means of control and the development of computational and numerical tools have allowed the introduction of new methods of characterization and modeling to study the effect of surface topography on the tribological performance of a hydrodynamic contact. These elements allowed [4] to demonstrate the potential of micro-irregularities to generate local hydrodynamic pressure, which allows significantly

* Corresponding author

increasing of the load-carrying capacity. Since then, several studies have been conducted in order to understand the physical mechanisms responsible for the increase in load capacity. Some studies attribute this elevation to the creation of a local pressure peak in the cavities [5,6], so the succession of texture judiciously arranged allows the construction of an evolutionary pressure field (global effect) due to the continuity of the local phenomenon. Therefore, the texture can be considered as a convergent zone [7], where the importance of optimizing the texture geometry to maximize their impact on the static characteristics of hydrodynamic contacts. A second theory attributes the positive impact of textures to convective inertia effects [8], while other authors show that inertia effects have a negative influence on hydrodynamic performance [9].

In 2016 Gropper et al. [10] conducted a comparative study of the results of research work concerning surface texturing in the hydrodynamic regime and they conclude that surface texturing allows the improvement of performances such as: load capacity, minimum lubricating film thickness, friction and wear.

Four years later, Vencl et al. [11] provided a review retracing the evolution of research that considers diverse surface textures and concluded that: the advantages of surface texturing can be better utilized when the surface texture design is optimized and applied to specific contact pairs. More recent studies are focused on optimizing the dimensions, shapes and positions of textures. For example, Dhiman [12] and Dhiman [13] studied the effect of positive sinusoidal half-wave and positive sinusoidal full-wave textures on the performance of a porous journal bearing by developing a model based on the Reynolds model and Darcy's law. It shows that partial texturing gives a better improvement in journal bearing characteristics compared to full texturing, and the optimized texture location was observed at an angle between 36° and 108° from the center line for the first texture type, and from 45° to 120° for the second type. Similarly, Hamdavi et al. [14] and Tauviqirrahman et al. [15] have shown that partial texturing has positive effects on the pressure and load carrying capacity of journal bearing with low relative eccentricity.

In 2017, Guo [16] studied the effect of spherical and cylindrical type texturing on an axial three-groove bearing, he concludes that texturing has a significant effect on the pressure in the lubricating film and the load carrying capacity when placed in the convergent zone of the journal bearing. One year later, Wang et al. [17] studied the effect of texture geometry, and he concludes that the convex spherical texture is better suited for plain bearings than the concave spherical texture. In another context, the incorporation of spherical textures at different locations (convergence zone and maximum pressure zone) of non-porous and porous journal bearings provides significant performance improvement [18]. A very recent study shows that the stability of a bearing can be increased by using cylindrical textures and that increasing the depth of the dimples has a significant effect on the critical mass [19]. Partial texturing of a bearing lubricated with micro polar and pseudo plastic fluid is very advantageous. It allows the bearing load to be increased and the coefficient of friction to be reduced [20].

The above studies are based on the assumption that the lubricant is Newtonian. However, practical lubrication applications show that oils containing viscosity additives have non-Newtonian rheological behavior. Their viscosity decreases when the shear rate to which they are subjected increases. During flow forces appear perpendicular to the shear plane [21], these forces could be proportional to the square of the rate of shear. Rosenberg [22] has shown experimentally that the minimum film thickness of a journal bearing lubricated by polymerized oil is more important than that measured with the pure mineral oils having the same viscosity. Therefore, classical continuum theory, which dismisses particle size, cannot accurately describe the flow of such fluids. Various models have been proposed in the literature to remedy this restriction and describe the behaviour of these complex fluids, known as couple stress fluids. These models incorporate stress moments in addition to conventional surface forces [23–25]. Of these theories, Stokes [23] theory is preferred in many studies because of its mathematical simplicity. It allows

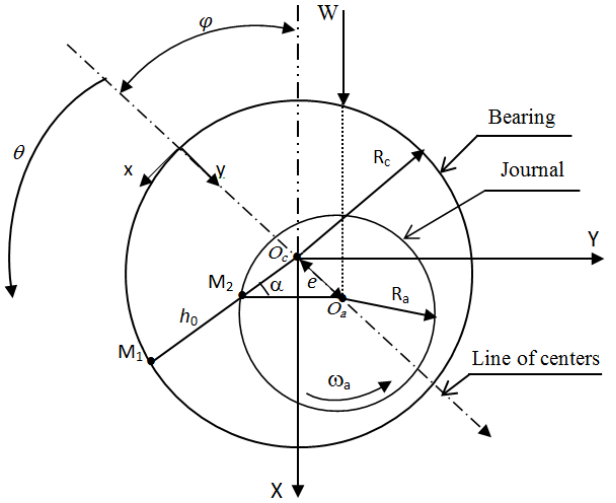

Figure 1. Journal bearing section.

taking into account the moving particle size and the couple stress due to the presence of viscosity additives. Several authors have used it to study problems of hydrodynamic lubrication [26–29]. It was demonstrated, that the static behavior of the journal bearing is significantly influenced by increasing the couple stress parameter. Similarly, Abass and Mahdi [30] showed that non-Newtonian fluids are beneficial for elliptical journal bearings with micro protrusions. However, the use of polar fluids to reduce the temperature in the contact was shown by Wang et al. [31].

This study investigates how surface texturing and couple stress fluid influence the hydrodynamic performance of journal bearings. Although surface texturing has been extensively studied with Newtonian fluids and couple stress models have demonstrated potential in representing non Newtonian lubricants, their combined impact remains largely unexplored.

The coupled effects of texture geometry and polar fluid behavior on global system performance are examined through numerical analysis, with a focus on pressure generation, Load-carrying capacity, friction factor, attitude angle, and side leakage flow.

2. Problem mathematical formulation

2.1. *Geometric model*

Figure 1 show section of a cylindrical bearing. In this case, the lubricant film thickness h_0 (m) in the y direction for a given angle θ is calculated by using this formula:

$$h_0 = C[1 + \varepsilon \cos\theta] \tag{1}$$

with

- $C = (R_c - R_a)$ is the radial clearance, R_c and R_a are the radius of the bearing and journal respectively,
- $\tilde{\varepsilon}$ is the relative eccentricity ($\tilde{\varepsilon} = e/C$) varying from 0 to 1,
- θ is the circumferential coordinate, measured trigonometrically from the line connecting the centers O_a and O_c.

This angular convention is used not only to locate textures on the surface of the bearing, but also to analyse pressure distribution and identify areas of convergence/divergence of the lubricating film based on the position around the shaft.

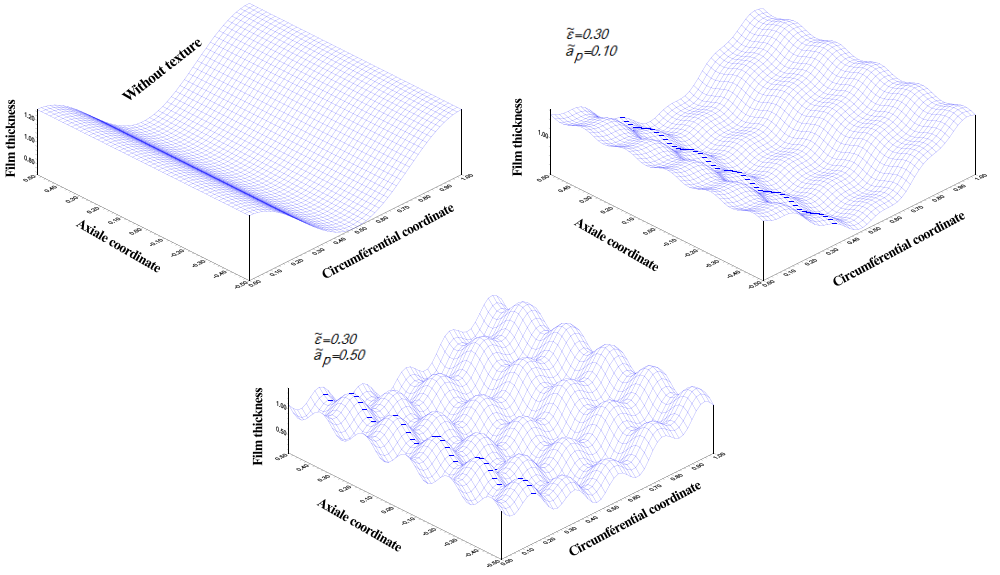

Figure 2. Lubricant film profile obtained for different values of asperity amplitude.

In this study, the positive sinusoidal half-wave profile was chosen for its mathematical simplicity, continuity and ability to provide a parametric representation of textured surfaces. It also allows clear parametric study, by independently controlling the amplitude and density of the asperity.

For this type of texture the lubricant film thickness h can be approached through the use of the formula proposed by Kango et al. [32]:

$$h = h_0 - \delta \tag{2}$$

$$\delta = -\left[\frac{2 * a_p}{\pi}\right]\left[\sum_{q=2,4,6\ldots\infty} \frac{\cos(q * B)}{q^2 - 1}\right] + \left[\frac{a_p}{\pi}\right] + \frac{a_p}{2}\sin(B) \tag{3}$$

with

- In the θ direction: $B = \pi R\theta/\lambda$ and $\lambda = 2\pi R/n_p$
- In the $\tilde{z}$ direction: $B = \pi z/\lambda$ and $\lambda = L/n_p$
- $\tilde{a}_p = a_p/C$

where, a_p, n_p and λ represent respectively: amplitude, number and wavelength of asperity, and δ is the film thickness variation caused by the presence of texture.

Figure 2 show the lubricant film profile obtained by using the chosen model.

2.2. *Governing equation*

The theoretical solution of a hydrodynamic lubrication problem requires the determination of the pressure field inside the lubricant film. The model used is based on the Stokes micro-continuum theory [23], the momentum equations and the continuity equation of an incompressible fluid with couple stress are:

$$\rho\frac{D\vec{V}}{Dt} = -\vec{\nabla}p + \rho\vec{A} + \frac{1}{2}\vec{\nabla}X(\rho\vec{E}) + \mu\vec{\nabla}^2\vec{V} - \eta\vec{\nabla}^4\vec{V} \tag{4}$$

$$\vec{\nabla}\cdot\vec{V} = 0, \tag{5}$$

where the vectors $\vec{V}$, $\vec{A}$ and $\vec{E}$ represent the velocity field, body force per unit mass, and body couple per unit mass, respectively; ρ represent the fluid density, P is the pressure, μ is the shear viscosity and η is a material constant responsible for the couple stress fluid property.

In case of steady state incompressible flow, when the body forces and body moments are ignored, and making the usual assumption of hydrodynamic lubrication applicable to thin films [33], the equation of motion are reduced to:

$$\begin{cases} \dfrac{\partial p}{\partial x} = \mu \dfrac{\partial^2 u}{\partial y^2} - \eta \dfrac{\partial^4 u}{\partial y^4} \\ \dfrac{\partial p}{\partial y} = 0 \\ \dfrac{\partial p}{\partial z} = \mu \dfrac{\partial^2 w}{\partial y^2} - \eta \dfrac{\partial^4 w}{\partial y^4}, \end{cases} \tag{6}$$

where u and w are the velocity components in the x and z direction.

Then, as descripted in [26], a modified Reynolds equation based on a couple stress models can be obtained by introducing the following dimensionless variables:

$$\theta = \frac{x}{R}; \quad \tilde{z} = \frac{z}{L}; \quad \tilde{h} = \frac{h}{C}; \quad \tilde{l} = \frac{l}{C}; \quad \tilde{p} = \frac{PC^2}{\mu\omega_a R^2}; \quad \tilde{G}(\tilde{h},\tilde{l}) = \frac{G(h,l)}{C^3}.$$

The dimensionless form of modified Reynolds equation can be given as:

$$\frac{\partial}{\partial\theta}\left[\tilde{G}(\tilde{h},\tilde{l})\frac{\partial\tilde{p}}{\partial\theta}\right] + \left[\frac{R}{L}\right]^2 \frac{\partial}{\partial\tilde{z}}\left[\tilde{G}(\tilde{h},\tilde{l})\frac{\partial\tilde{p}}{\partial\tilde{z}}\right] = 6\frac{\partial\tilde{h}}{\partial\theta} \tag{7}$$

$$\tilde{G}(\tilde{h},\tilde{l}) = \tilde{h}^3 - 12\tilde{l}^2\tilde{h} + 24\tilde{l}^3 \tanh\left[\frac{\tilde{h}}{2\tilde{l}}\right]. \tag{8}$$

In the previous equation ω_a is the velocity of journal and $l = (\eta/\mu)^{1/2}$ is the couple stress parameter. It can vary from 0 to 1.

This variation illustrates the transition from Newtonian behavior ($\tilde{l} = 0$) to that of non-Newtonian lubricants.

Physically, it represents the relative length of the molecular chains in additives that are added to the base oil to enhance lubricant performance, such as improving viscosity.

The deterministic approach is employed to solve the Reynolds equation. Unlike the stochastic method, which introduces empirical flow factors to account for surface texture effects, the deterministic approach models these effects directly by incorporating the surface texture into the fluid film thickness equation through explicit geometric representation.

2.3. *Boundary conditions*

The Reynolds boundary conditions are used. They respect flow continuity and film rupture. They assume that for an unknown abscissa θ_c, the pressure and pressure gradient become zero.

$$\tilde{p}[\theta, \tilde{z} = \pm\tfrac{1}{2}] = 0 \tag{9}$$

$$\tilde{p} = \frac{\partial\tilde{p}}{\partial\theta} = 0; \quad \text{for } \theta = \theta_c. \tag{10}$$

However, these conditions do not satisfy film reformation. Their use requires the determination of an additional unknown, θ_c, which is the cavitation angle. Thus, an unknown boundary between the active and inactive zones of the lubricant film is defined by $\theta = \theta_c$. It is assumed that the abscissa of the film reformation is known and coincides with ($\theta = 0$).

The respect of these conditions is made by the application of the Cristopherson algorithm [34]. This algorithm allows the suppression of negative pressure terms during the computations and the study will be limited to the active zone of the bearing.

Thus, the determination of the static pressure distribution in the lubricant film for a given position of the shaft in the bearing allows the calculation of the static performance of the bearing such as: load-carrying capacity, attitude angle, Sommerfeld number, friction factor, and side leakage flow.

2.4. *Static characteristics*

- The components of the dimensionless load carrying capacity are expressed by:

$$\begin{cases} \tilde{F}_1 = \displaystyle\int_{-\frac{1}{2}}^{\frac{1}{2}} \int_0^{2\pi} \tilde{p}(\theta,\tilde{z}) \cos\theta \, \mathrm{d}\theta \, \mathrm{d}\tilde{z} \\ \tilde{F}_2 = \displaystyle\int_{-\frac{1}{2}}^{\frac{1}{2}} \int_0^{2\pi} \tilde{p}(\theta,\tilde{z}) \sin\theta \, \mathrm{d}\theta \, \mathrm{d}\tilde{z}. \end{cases} \tag{11}$$

It is from these two relationships that we can determine the following expressions:

- Static attitude angle:

$$\varphi = \tan^{-1}\left[-\frac{\tilde{F}_2}{\tilde{F}_1}\right]. \tag{12}$$

- The resultant of load carrying capacity:

$$\tilde{F} = \sqrt{\tilde{F}_1^2 + \tilde{F}_2^2}. \tag{13}$$

- The Sommerfeld number:

$$S = \frac{1}{\pi \tilde{F}}. \tag{14}$$

- The friction couple is obtained by integrating the shear stresses at the shaft surface ($y = h$):

$$T_a = R \int_s [\sigma_{xy}]_{y=0,h} \, \mathrm{d}s. \tag{15}$$

In laminar flow, the expression for shear stress in a couple stress fluids is given by:

$$[\sigma_{xy}]_{y=0,h} = \mu \left.\frac{\partial u}{\partial y}\right|_{y=0,h} + \underbrace{\eta \left.\frac{\partial^3 u}{\partial y^3}\right|_{y=0,h}}_{=0} = \mu\left(\frac{\omega_a R}{h} \mp \frac{1}{2\mu R}\frac{\partial P}{\partial \theta}\left(h - 2l\tanh\left(\frac{h}{2l}\right)\right)\right). \tag{16}$$

The non dimensionless friction couple on the journal is written as:

$$\tilde{T}_a = \int_{-\frac{1}{2}}^{\frac{1}{2}} \int_0^{2\pi} \left[\frac{1}{\tilde{h}} + \frac{1}{2}\frac{\partial \tilde{p}}{\partial \theta}\left(\tilde{h} - 2\tilde{l}\tanh\left(\frac{\tilde{h}}{2\tilde{l}}\right)\right)\right] \mathrm{d}\theta \, \mathrm{d}\tilde{z}. \tag{17}$$

- The friction factor is defined as:

$$\tilde{f} = \frac{\tilde{T}_a}{\tilde{F}}. \tag{18}$$

- Side leakage flow:

$$\tilde{Q} = -\frac{1}{12}\int_0^{2\pi} \tilde{h}^3 \frac{\partial \tilde{p}}{\partial \tilde{z}} \, \mathrm{d}\theta + \tilde{l}^2 \int_0^{2\pi} \frac{\partial \tilde{p}}{\partial \tilde{z}}\left[\tilde{h} - 2\tilde{l}\tanh\left(\frac{\tilde{h}}{2\tilde{l}}\right)\right] \mathrm{d}\theta. \tag{19}$$

3. Numerical analysis

The governing equations are solved numerically using the centered finite-difference method. The field of solution is divided in to grid spacing ($N\ X\ M$) each of a mesh size is $\Delta\theta X \Delta\tilde{z}$.

The discrete system of equations obtained is solved using the Gauss–Seidel method with the over relaxation coefficient Ω varying from 1 to 2. Applying this algorithm, we can write:

$$\tilde{p}_{ij}^{(k+1)} = (1-\Omega)\tilde{p}_{ij}^{(k)} + \Omega\left[a_{ij}\tilde{p}_{i+1,j}^{(k)} + b_{ij}\tilde{p}_{i-1,j}^{(k+1)} + C_{ij}\tilde{p}_{i,j+1}^{(k')} + d_{ij}\tilde{p}_{i,j-1}^{(k+1)} + e_{ij}\right] \tag{20}$$

with

$$a_{ij} = \left[\frac{\tilde{G}}{\Delta\theta^2} + \frac{1}{2\Delta\theta}\left(\frac{\partial\tilde{G}}{\partial\theta}\right)_{ij}\right]\frac{1}{F_{ij}}; \quad b_{ij} = \left[\frac{\tilde{G}}{\Delta\theta^2} - \frac{1}{2\Delta\theta}\left(\frac{\partial\tilde{G}}{\partial\theta}\right)_{ij}\right]\frac{1}{F_{ij}};$$

$$c_{ij} = \left[\frac{\tilde{G}}{\Delta\tilde{z}^2} + \frac{1}{2\Delta z}\left(\frac{\partial\tilde{G}}{\partial\tilde{z}}\right)_{ij}\right]\frac{\lambda}{F_{ij}}; \quad d_{ij} = \left[\frac{\tilde{G}}{\Delta\tilde{z}^2} - \frac{1}{2\Delta z}\left(\frac{\partial\tilde{G}}{\partial\tilde{z}}\right)_{ij}\right]\frac{\lambda}{F_{ij}}; \quad e_{ij} = 6\left[\frac{\partial\tilde{h}}{\partial\theta}\right]_{ij}\frac{1}{F_{ij}};$$

$$F_{ij} = 2\tilde{G}\left[\frac{1}{\Delta\theta^2} + \frac{\lambda}{\Delta\tilde{z}^2}\right]; \quad \lambda = \left[\frac{R}{L}\right]^2,$$

where k is the iteration number, $\tilde{P}_{ij}$ is the dimensionless pressure in node (i, j), and a_{ij}, b_{ij}, c_{ij}, d_{ij}, e_{ij}, f_{ij} are the discretization coefficients.

Several mesh densities were tested to ensure grid-independent results, and a 600 × 100 grid was finally selected based on the convergence analysis presented in the Appendix A. The iterative process was considered converged when, at every computational point, the relative error between two successive iterations dropped below a tolerance of 10^{-6}.

4. Validation

To validate the numerical method developed for the study of the influence of surface texturing on the static characteristics of a bearing lubricated with a polar fluid, we compared our results with those obtained by Constantinescu et al. [35]. The compared parameters are: the attitude angle and the Sommerfeld number. The calculations were performed for a Newtonian fluid ($\tilde{l} = 0$) for three values of relative eccentricity ($\tilde{\varepsilon} = 0.0962; 0.5374; 0.8349$). The results obtained are reported in Table 1.

The 30% deviation observed at low eccentricity required further mesh-sensitivity analyses (Appendix B), which confirmed that grid refinement has a negligible effect on the results. The deviation is attributed to the low-load operating regime, which is characterized by a thicker lubricant film and lower pressure, making the load-carrying capacity sensitive to small variations. It is also attributed to the higher experimental uncertainty typically associated with such conditions.

However, the numerical model shows good agreement with the results of Constantinescu et al. for medium and high eccentricity ratios.

Table 1. Comparison of theoretical results obtained for a journal bearing of finite length ($R/L = 0.5$)

$\tilde{\varepsilon}$	0.0962	0.5374	0.8349	
S	1.03540	0.1549	0.0345	Reference results
	1.35970	0.1555	0.0352	Present work
ϕ (deg)	84.03	56.07	33.03	Reference results
	84.09	56.18	33.52	Present work

5. Results and discussion

A parametric study was conducted to evaluate the combined effects of surface texturing and rheology flow on the static performance of a hydrodynamic bearing with finite length ($R/L = 0.5$), lubricated with a polar fluid where the dimensionless couple stress parameter vary from 0.0 to 0.50 ($\tilde{l} = 0.0$ case of Newtonian fluid).

The solutions have been obtained for some combinations of relative amplitude of texture (0.0; 0.10; 0.20; 0.35) and number of asperity (10; 30; 60; 100). Noting that the relative amplitude of texture ($\tilde{a}_p = 0.0$) correspond to the smooth bearing case.

The circumferential distributions of the static pressure are determined for two values of the static relative eccentricity ($\tilde{\varepsilon} = 0.5$ and 0.9) along the median section of the bearing. In addition, the static performances were determined for a relative eccentricity ratio varying from 0.05 to 0.9.

To illustrate the combined effect of the textured surfaces and the couple stress parameter on the static hydrodynamic pressure field, the results obtained for a hydrodynamic textured bearing lubricated with a polar fluid are compared to those of a hydrodynamic journal bearing lubricated by a Newtonian fluid.

5.1. *Static hydrodynamic pressure*

In order to illustrate the combined effect of the textured surfaces and the couple stress parameter on the static hydrodynamic pressure field, the results obtained for a hydrodynamic textured bearing lubricated with a polar fluid are compared to those of a hydrodynamic journal bearing lubricated by a Newtonian fluid.

5.1.1. *Texture amplitude effects*

In order to analyze the effect of the texture amplitude on the static pressure in the lubricant film, the number of periods was fixed at 60, varying the value of the texture amplitude between 0.10 and 0.35.

Figure 3 shows the two-dimensional circumferential variations of dimensionless static pressures in the median section of the hydrodynamic bearing for different values of $\tilde{a}_p$ and $\tilde{l}$, with $n_p = 60$. It clearly shows that an increase in texturing amplitude leads to a rise in maximum pressure, for both Newtonian and non-Newtonian lubricants.

The effect of texturing amplitude becomes more pronounced as the couple stress parameter increases. An analysis of the variations reveals that the sensitivity of maximum pressure to texturing amplitude is significantly enhanced for high values of the couple stress parameter and relative eccentricity ratio ($\tilde{l} = 0.50$ and $\tilde{\varepsilon} = 0.9$). Therefore, the effect of texturing amplitude is more pronounced at high values of the couple stress.

The analysis of the static pressure distributions indicates that increasing the texture amplitude generates local pressure peaks in the convergence zones formed by the surface asperities, in agreement with previous studies [5,6]. The regular and continuous arrangement of textures enables the superposition of these local effects, leading to a globally increasing pressure field that reflects the cumulative influence of the surface texture. Moreover, the use of a polar lubricant enhances pressure development.

5.1.2. *Texture number periods effects*

In order to show the effect of texture number on the static pressure in the lubricant film, the texture amplitude was set to 0.1, varying the texture number value between 10 and 100.

Figure 4 presents the circumferential variations of dimensionless static pressure in the median section of the bearing. Analysis of these profiles shows that: the effect of the number of texture

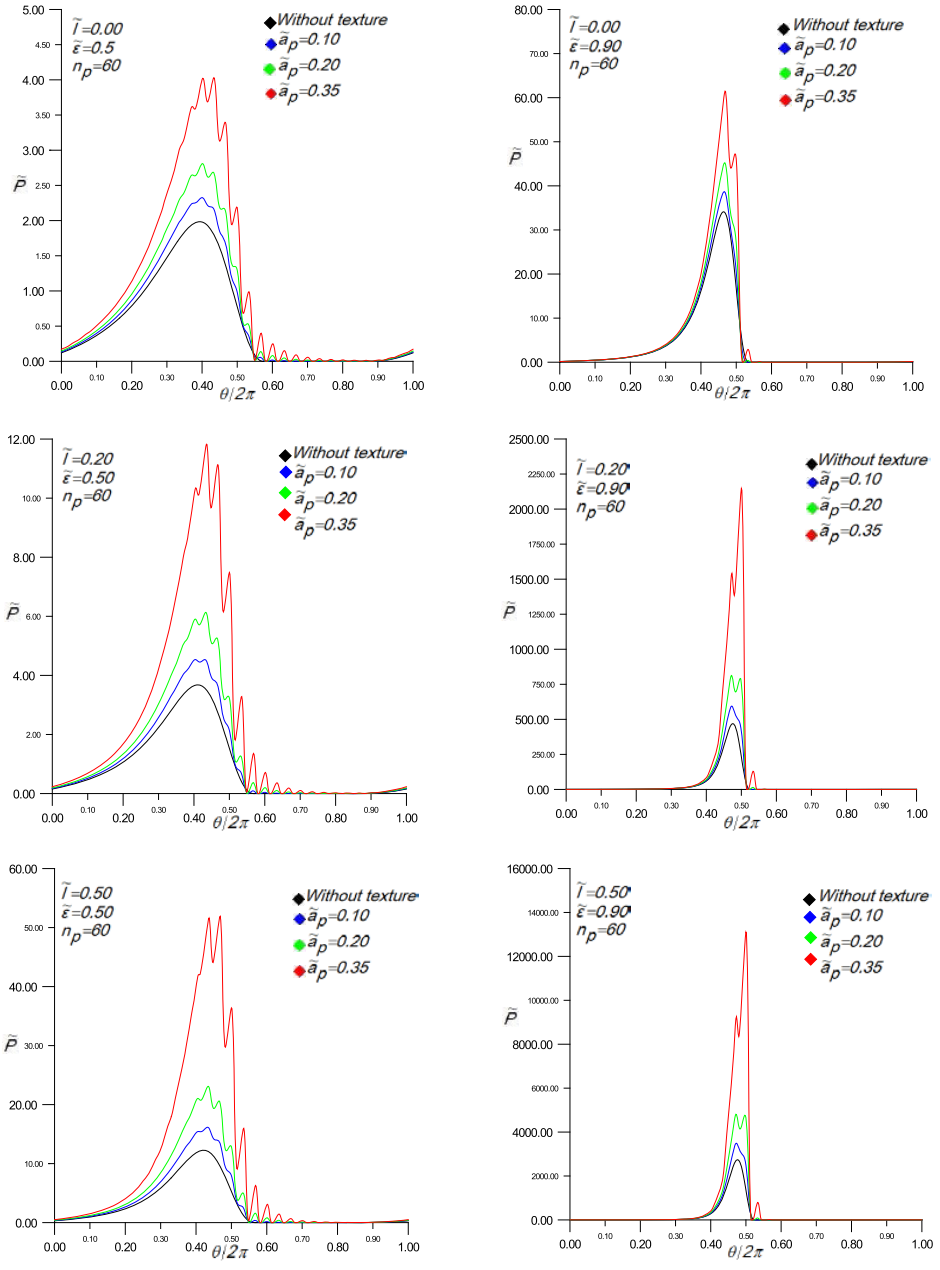

Figure 3. Circumferential static pressure in journal bearing for different value of $\tilde{a}_p$ and $\tilde{l}$.

periods on the maximum pressure is positive. It also increases with increasing of couple stress parameter and relative eccentricity ratio.

An increase in texture density, characterized by a higher number of textures, creates additional converging zones, which induce local pressure peaks. The superposition of these localized effects enhances the global pressure field. This effect is further amplified by the use of a couple stress lubricants.

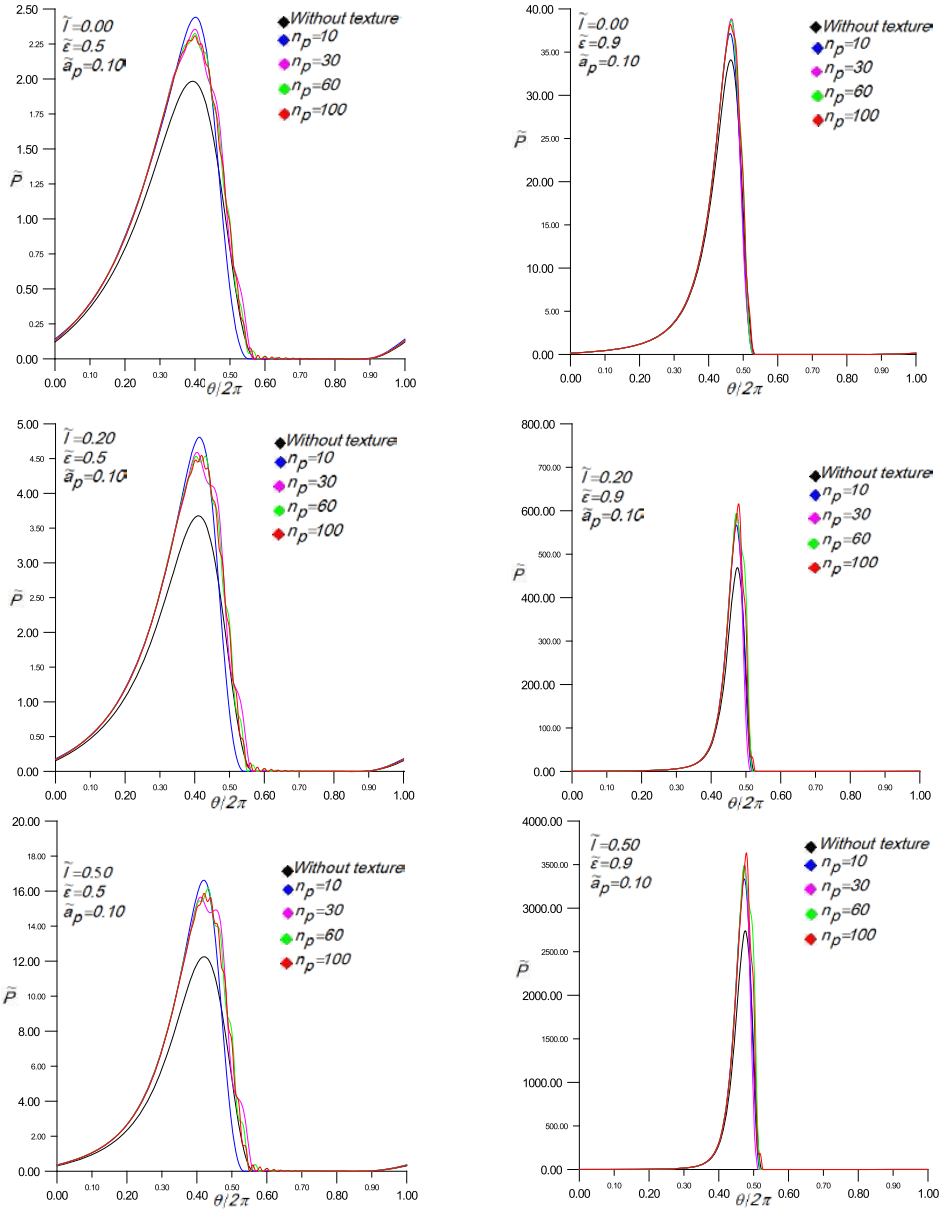

Figure 4. Circumferential static pressure in journal bearing for different value of n_p and $\tilde{l}$.

5.2. *Static characteristics of journal bearing*

Figure 5(a–d) presents static characteristics variation of the hydrodynamic bearing with relative eccentricity for different values of amplitude texture. The obtained results show:

For a given value of relative eccentricity ratio, the load-carrying capacity increases with increasing of the amplitude of textures (Figure 4a). This increase is more relevant for bearings lubricated with non-Newtonian fluids and highly loaded. While the attitude angle and friction number show a diminution with the increase of the amplitude (Figure 5b,c), which becomes more

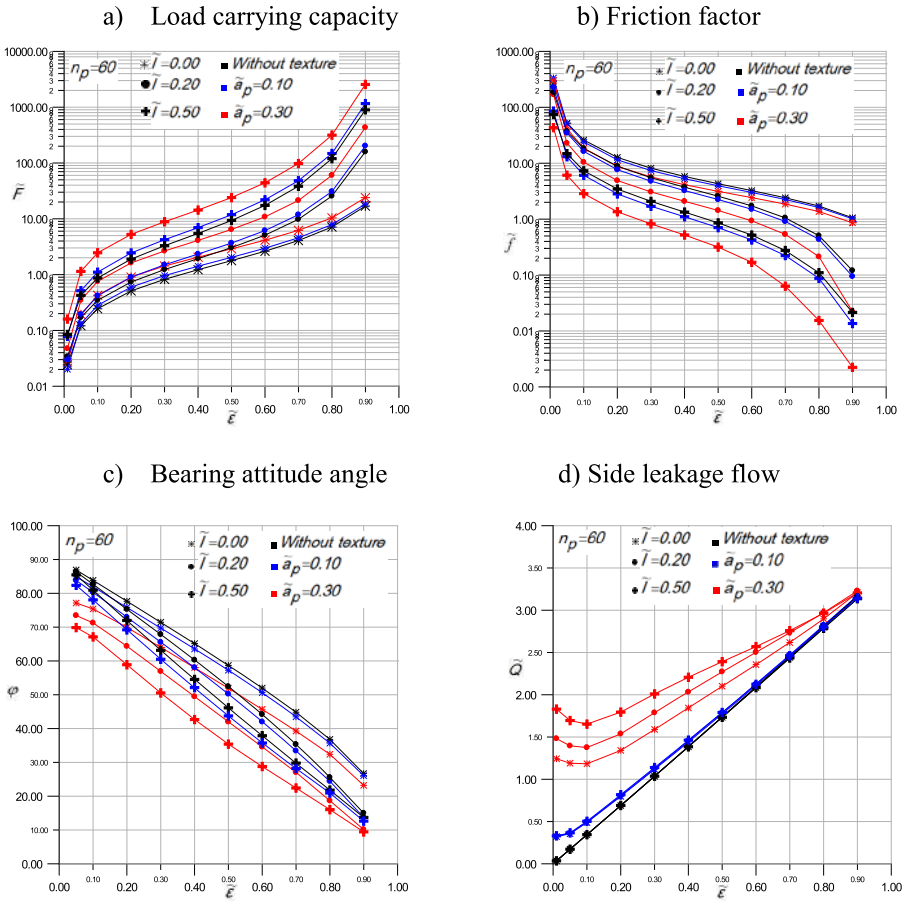

Figure 5. Dimensionless static characteristics for various values of $\tilde{a}_p$ and $\tilde{l}$.

important for the high values of couple stress parameter and those of the relative eccentricity ratio. It can be concluded that the combination of surface texturing and polar fluids improves the bearing load capacity and reduces frictional losses in the hydrodynamic contacts.

At low relative eccentricity ratio the side leakage flow has a significant increase with the increase of the amplitude (Figure 5d). This effect is more evident for high values of the couple stresses parameter. Therefore, the association of textured surfaces and polar fluids has a positive effect on the side leakage flow at low relative eccentricity ratio, which assures a good lubricant supply. This constant regeneration of lubricant in the contact area helps to maintain a stable and continuous lubricating film.

6. Conclusion

The parametric analysis demonstrated that both surface texturing with continuous geometry and lubrication with polar fluids have a significant influence on the static performance of a highly loaded hydrodynamic journal bearing. Increasing the texture amplitude and density creates converging zones where local pressure peaks are generated, which results in a net increase in the

static pressure. The influence on the side leakage flow is limited; however, a noticeable positive effect is observed at low eccentricity ratios.

Compared with the plain bearing lubricated by Newtonian oils, the textured bearing lubricated by couple stress fluids allows:

- High increase in load-carrying capacity and static pressure peak in the lubricating film, especially for high values of the couple stress parameter and relative eccentricity.
- Reduction in the attitude angle and friction factor in the contact improving energy efficiency and tribological system stability.
- Provide a good lubricant supply, particularly beneficial for low load bearings. This provides more reliable operation and reduces the risk of failing due to insufficient lubrication.

These results confirm the importance of optimizing surface textures and selecting the appropriate lubricating fluids to improve the performance of hydrodynamic bearings under extreme operating conditions. They also open up interesting prospects for the design of more efficient and energy-saving tribological systems, particularly in industrial applications where performance and durability requirements are becoming increasingly stringent.

Declaration of interests

The authors do not work for, advise, own shares in, or receive funds from any organization that could benefit from this article, and have declared no affiliations other than their research organizations.

Nomenclature

$\vec{A}$	Body force per unit mass, (N·kg^{-1})
a_p	Amplitude of asperity, (m)
$\tilde{a}_p$	Dimensionless amplitude of asperity
C	Radial clearance, (m)
$\vec{E}$	Body couple per unit mass, (N·m·kg^{-1})
e	Eccentricity, $e = \lvert\vec{o_a o_c}\rvert$, (m)
F	Load carrying capacity, (N)
$\tilde{F}$	Dimensionless load carrying capacity, $\tilde{F} = \sqrt{\tilde{F}_1^2 + \tilde{F}_2^2}$
F_1, F_2	Load carrying capacity components, (N)
$\tilde{F}_1, \tilde{F}_2$	Dimensionless load carrying capacity components, $(\tilde{F}_1, \tilde{F}_2) = (F_1, F_2)/(\mu\omega_a RL(R/C)^2)$
$\tilde{f}$	Friction number, $\tilde{f} = \tilde{C}_a/\tilde{F}$
h_0	Film thickness without texture, (m)
h	Film thickness with texture, (m)
$\tilde{h}$	Dimensionless film thickness with texture, $\tilde{h} = h/C$
L	Bearing length, (m)
l	Characteristics length of the additives, $l = \sqrt{\eta/\mu}$, (m)
$\tilde{l}$	Dimensionless couple stress parameter, $\tilde{l} = l/C$
n_p	Number of asperity
o_a	Center of the journal
o_c	Center of the bearing
p	Lubricant pressure, (Pa)
$\tilde{p}$	Dimensionless lubricant pressure, $\tilde{p} = p/(\mu\omega_a(R/C)^2)$
Q	Side leakage flow, (m^3·s^{-1})

$\tilde{Q}$	Dimensionless side leakage flow, $\tilde{Q} = LQ/(C\omega_a R^3)$
R_a	Journal radius, (m)
R_c	Bearing radius, (m)
S	Sommerfeld number, $S = (\mu\omega_a RL(R/C)^2)/\pi F$
T_a	Friction couple, (N/m)
$\tilde{T}_a$	Dimensionless friction couple, $(\tilde{T}_a) = (C/(\mu\omega_a R^3 L))(T_a)$
t	Temps, (s)
$\vec{V}$	Velocity field, (m/s)
u	The velocity components in the x direction, (m/s)
w	The velocity components in the z direction, (m/s)
x, y, z	Axial coordinates of bearing, (m)
$\tilde{z}$	Dimensionless axial coordinate of bearing, $\tilde{z} = z/L$
δ	Film thickness variation caused by the presence of texture, (m)
$\tilde{\varepsilon}$	Relative eccentricity, $\tilde{\varepsilon} = e/C$
η	Material constant responsible for the couple stress fluid property, (N·s)
θ	Circumferential coordinate starting from the line of the centers, $\theta = x/R$, (rad)
θ_c	Cavitation angle, (rad)
μ	Lubricant dynamic viscosity, (Pa·s)
ρ	Lubricant density, (kg/m^3)
ϕ	Attitude angle, (rad)
Ω	Over relaxation coefficient, $1 < \Omega < 2$
λ	Wavelength of asperity, (m)
ω_a	Journal angular velocity, (rad/s)
∇	Gradient operator
$\sim$	On top of a variable denotes dimensionless quantity
X	Vector (cross) product

Appendix A. Numerical experiment and mesh convergence analysis

A mesh convergence study was carried out to ensure the reliability and accuracy of the numerical results. This step is an essential part of validating the numerical model and aims to verify that the computed quantities no longer depend significantly on mesh refinement.

Several meshes with increasing densities were tested and the results were compared using a relative variation criterion. The objective of this numerical experiment is to determine the optimal mesh that balances computational cost with solution accuracy and ensures numerical stability.

Table 2 presents the results obtained from the computational code, illustrating the variation of the journal bearing's characteristic quantities with mesh refinement.

The influence of mesh refinement on numerical stability was evaluated using a relative variation criterion defined as

$$\Delta_i(\%) = \frac{|\psi_{M_{i+1}} - \psi_{M_i}|}{\psi_{M_{i+1}}} \times 100,$$

where $\Delta_i(\%)$ is the relative variation in percent of the physical quantity ψ between two successive meshes M_i and M_{i+1}; ψ_{M_i} and $\psi_{M_{i+1}}$ denote the values of the considered quantity obtained with meshes M_i and M_{i+1} respectively; M_i considered mesh level, defined by a specific number of axial and circumferential divisions; M_{i+1} represent a progressive refinement of the computational domain used for the numerical convergence analysis.

This criterion evaluates the numerical stability and convergence of the results with respect to mesh refinement. The corresponding results are summarized in Table 3.

Table 2. Influence of mesh refinement on the computed bearing performance characteristics

Parameters	$N_\theta \times N_z$	Calculation time CPU (s)	Maximum pressure	Load-carrying capacity	Attitude angle
$\varepsilon = 0.1$, $\tilde{l} = 0.0$, $\tilde{a}_p = 0.0$, $n_p = 0.0$	$M1 = 150 \times 25$	7.08	0.22	0.24	83.84
	$M2 = 300 \times 50$	7.80	0.22	0.24	83.84
	$M3 = 600 \times 100$	30.88	0.22	0.24	83.84
	$M4 = 1200 \times 200$	117.39	0.22	0.24	83.84
$\varepsilon = 0.9$, $\tilde{l} = 0.0$, $\tilde{a}_p = 0.0$, $n_p = 0.0$	$M1 = 150 \times 25$	4.84	34.03	16.77	26.66
	$M2 = 300 \times 50$	9.91	34.10	16.85	26.69
	$M3 = 600 \times 100$	24.97	34.10	16.87	26.70
	$M4 = 1200 \times 200$	133.14	34.10	16.88	26.70
$\varepsilon = 0.1$, $\tilde{l} = 0.5$, $\tilde{a}_p = 0.0$, $n_p = 0.0$	$M1 = 150 \times 25$	4.96	0.81	0.87	80.94
	$M2 = 300 \times 50$	6.88	0.81	0.87	80.93
	$M3 = 600 \times 100$	21.83	0.81	0.87	80.93
	$M4 = 1200 \times 200$	126.40	0.81	0.87	80.93
$\varepsilon = 0.9$, $\tilde{l} = 0.5$, $\tilde{a}_p = 0.0$, $n_p = 0.0$	$M1 = 150 \times 25$	6.05	2690.84	871.34	13.60
	$M2 = 300 \times 50$	7.14	2735.62	891.07	13.68
	$M3 = 600 \times 100$	29.16	2739.58	895.41	13.71
	$M4 = 1200 \times 200$	131.45	2740.97	896.51	13.72
$\varepsilon = 0.5$, $\tilde{l} = 0.0$, $\tilde{a}_p = 0.1$, $n_p = 10$	$M1 = 150 \times 25$	6.74	2.45	1.10	60.07
	$M2 = 300 \times 50$	11.89	2.44	1.10	60.08
	$M3 = 600 \times 100$	26.09	2.44	1.10	60.08
	$M4 = 1200 \times 200$	110.24	2.44	1.10	60.08
$\varepsilon = 0.5$, $\tilde{l} = 0.5$, $\tilde{a}_p = 0.1$, $n_p = 10$	$M1 = 150 \times 25$	5.81	16.80	11.13	48.25
	$M2 = 300 \times 50$	6.61	16.71	11.12	48.30
	$M3 = 600 \times 100$	27.75	16.70	11.11	48.31
	$M4 = 1200 \times 200$	146.68	16.69	11.11	48.31
$\varepsilon = 0.9$, $\tilde{l} = 0.0$, $\tilde{a}_p = 0.35$, $n_p = 100$	$M1 = 150 \times 25$	4.41	49.46	21.39	25.20
	$M2 = 300 \times 50$	8.49	60.66	25.65	22.48
	$M3 = 600 \times 100$	32.15	58.06	25.08	22.77
	$M4 = 1200 \times 200$	158.38	59.15	25.49	22.65
$\varepsilon = 0.9$, $\tilde{l} = 0.50$, $\tilde{a}_p = 0.35$, $n_p = 100$	$M1 = 150 \times 25$	5.49	7887.24	1788.28	10.50
	$M2 = 300 \times 50$	10.96	12119.53	2987.36	9.04
	$M3 = 600 \times 100$	37.67	10528.61	2678.27	9.79
	$M4 = 1200 \times 200$	171.81	10830.71	2710.44	9.94

The comparison between mesh levels shows that the computed results are practically insensitive to further refinement, with differences between the (600×100) and (1200×200) meshes are under 1% for all cases and not exceeding 3% for the case with: $\varepsilon = 0.9$, $\tilde{l} = 0.50$, $\tilde{a}_p = 0.35$, $n_p = 100$. This consistency confirms the numerical robustness of the model and the results' validity.

Therefore, the (600×100) mesh was selected as the optimal configuration, as it provides an appropriate balance between computational accuracy and cost.

Table 3. Relative variations of maximum pressure, load-carrying capacity, and attitude angle

Parameters	Maximum pressure $\tilde{P}_{\max}$			Load-carrying capacity $\tilde{F}$			Attitude angle φ		
	Δ_1 (%)	Δ_2 (%)	Δ_3 (%)	Δ_1 (%)	Δ_2 (%)	Δ_3 (%)	Δ_1 (%)	Δ_2 (%)	Δ_3 (%)
$\varepsilon = 0.1$, $\tilde{l} = 0.0$, $\tilde{a}_p = 0.0$, $n_p = 0.0$	0.00	0.00	0.00	0.00	0.00	0.00	0.00	0.00	0.00
$\varepsilon = 0.9$, $\tilde{l} = 0.0$, $\tilde{a}_p = 0.0$, $n_p = 0.0$	0.20	0.00	0.00	0.47	0.11	0.05	0.11	0.04	0.00
$\varepsilon = 0.1$, $\tilde{l} = 0.5$, $\tilde{a}_p = 0.0$, $n_p = 0.0$	0.00	0.00	0.00	0.00	0.00	0.00	0.01	0.00	0.00
$\varepsilon = 0.9$, $\tilde{l} = 0.5$, $\tilde{a}_p = 0.0$, $n_p = 0.0$	1.64	0.14	0.05	2.21	0.48	0.12	0.58	0.22	0.07
$\varepsilon = 0.5$, $\tilde{l} = 0.0$, $\tilde{a}_p = 0.1$, $n_p = 10$	0.41	0.00	0.00	0.00	0.00	0.00	0.02	0.00	0.00
$\varepsilon = 0.5$, $\tilde{l} = 0.5$, $\tilde{a}_p = 0.1$, $n_p = 10$	0.54	0.06	0.06	0.09	0.09	0.00	0.10	0.02	0.00
$\varepsilon = 0.9$, $\tilde{l} = 0.0$, $\tilde{a}_p = 0.35$, $n_p = 100$	18.46	4.48	1.84	16.60	2.27	1.60	12.09	1.27	0.52
$\varepsilon = 0.9$, $\tilde{l} = 0.50$, $\tilde{a}_p = 0.35$, $n_p = 100$	34.92	15.11	2.79	40.14	11.54	1.19	16.15	7.67	1.51

Appendix B. Low-eccentricity case: additional numerical tests

Table 4 presents the results of additional numerical tests for the low-eccentricity case. These results highlight the influence of mesh refinement on the computed bearing performance parameters.

Table 4. Numerical results for the low-eccentricity case

Parameters	$N_\theta \times N_z$	Maximum pressure	Load-carrying capacity	Attitude angle	Sommerfeld number
$\varepsilon = 0.0962$, $\tilde{l} = 0.0$, $\tilde{a}_p = 0.0$, $n_p = 0.0$	$M1 = 150 \times 25$	0.22	0.23	84.07	1.36
	$M2 = 300 \times 50$	0.22	0.23	84.07	1.36
	$M3 = 600 \times 100$	0.22	0.23	84.07	1.36
	$M4 = 1200 \times 200$	0.22	0.23	84.07	1.36

References

[1] O. Reynolds, "On the theory of lubrication and its application to Mr. Beauchamp Tower's experiments, including an experimental determination of the viscosity of olive oil", *Phil. Trans. R. Soc. Lond.* **177** (1886), pp. 157–234.

[2] K. Serpin, *Anti-friction texturing of the cylindrical bearings of crankshafts*, Process Engineering, ENSAM, 2017. Online at https://pastel.hal.science/tel-01692997v1 (accessed on December 1, 2023). French.

[3] A. Vencl, L. Ivanović, B. S. Stojanović, E. Zadorozhnaya, S. Miladinović and P. Svoboda, "Surface texturing for tribological applications: a review", in *16th International Conference on Tribology*, Faculty of Engineering University of Kragujevac, Serbian Tribology Society, 2019, pp. 227–239.

[4] I. Etsion, "State of the art in laser surface texturing", *J. Tribol.* **127** (2005), no. 1, pp. 248–253.

[5] D. B. Hamilton, J. A. Walowit and C. M. Allen, "A theory of lubrication by micro-irregularities", *J. Basic Eng.* **88** (1966), no. 1, pp. 177–185.

[6] V. Brizmer, Y. Kligerman and I. Etsion, "A laser surface textured parallel thrust bearing", *Tribol. Trans.* **46** (2003), no. 3, pp. 397–403.

[7] M. Fowell, A. V. Olver, A. D. Gosman, H. A. Spikes and I. Pegg, "Entrainment and inlet suction: two mechanisms of hydrodynamic lubrication in textured bearings", *J. Tribol.* **129** (2006), no. 2, pp. 336–347.

[8] M. D. Pascovici, T. Cicone, M. Fillon and M. B. Dobrica, "Analytical investigation of a partially textured parallel slider", *Proc. Inst. Mech. Eng. J: J Eng. Tribol.* **223** (2008), no. 2, pp. 151–158.

[9] M. Arghir, N. Roucou, M. Helene and J. Frene, "Theoretical analysis of the incompressible laminar flow in a macro-roughness cell", *J. Tribol.* **125** (2003), no. 2, pp. 309–318.

[10] M. B. Dobrica and M. Fillon, "About the validity of Reynolds equation and inertia effects in textured sliders of infinite width", *Proc. Inst. Mech. Eng. J: J Eng. Tribol.* **223** (2008), no. 1, pp. 69–78.

[11] D. Gropper, L. Wang and T. J. Harvey, "Hydrodynamic lubrication of textured surfaces: a review of modeling techniques and key findings", *Tribol. Int.* **94** (2015), pp. 509–529.

[12] Y. Dhiman, "Investigation on the influence of positive half wave type textures on the performance of porous journal bearing", *Int. J. Appl. Eng. Technol.* **6** (2016), pp. 81–88. Online at https : / / www . cibtech . org / J - ENGINEERING - TECHNOLOGY / PUBLICATIONS / 2016 / VOL - 6 - NO - 3 / 11 - JET - 011 - YOGESH - INVESTIGATION - BEARING.pdf. ISSN: 2277-212X.

[13] S. Dhiman, "Studies on the effect of positive full wave type transverse textures on the performance of porous journal bearings", *Int. J. Appl. Eng. Technol.* **6** (2016), pp. 89–96. Online at https : / / www . cibtech . org / J - ENGINEERING - TECHNOLOGY / PUBLICATIONS / 2016 / VOL - 6 - NO - 3 / 12 - JET - 012 - DHIMAN - STUDIES - BEARINGS.pdf. ISSN: 2277-212X.

[14] S. Hamdavi, H. H. Ya and T. V. V. L. N. Rao, "Effect of surface texturing on hydrodynamic performance of journal bearings", *ARPN J. Eng. Appl. Sci.* **11** (2016), no. 01, pp. 172–176. Online at http://www.arpnjournals.org/jeas/research_papers/rp_2016/jeas_0116_3314.pdf. ISSN: 1819-6608.

[15] J. Tauviqirrahman Jamari, B. Setiyana, M. Muchammad and D. Prabowo, "Performance analysis of a new design concept of journal bearing with surface roughness", *J. Tribol.* **38** (2023), pp. 1–18. Online at https://jurnaltribologi.mytribos.org/v38/JT-38-1-18.pdf.

[16] B. Guo, "Optimal surface texture design of journal bearing with axial grooves", *Int. J. Heat Technol.* **35** (2017), no. 2, pp. 267–272.

[17] J. Wang, J. Zhang, J. Lin and L. Ma, "Study on lubrication performance of journal bearing with multiple texture distributions", *Appl. Sci.* **8** (2018), no. 2, article no. 244.

[18] N. Sharma and S. Kango, "Influence of high permeability parameter on the performance of textured porous journal bearings", *Tribol. Indust.* **42** (2020), no. 3, pp. 370–381.

[19] S. Wang, Q. Wan and Z. Xiong, "Stability analysis of hydrodynamic journal bearing with surface texture", in *International Conference on Machine Learning and Intelligent Systems Engineering (MLISE), Chongqing, China*, 2021, pp. 499–502.

[20] T. V. V. L. N. Rao, A. M. A. Rani, N. M. Mohamed, H. H. Ya, M. Awang and F. M. Hashim, *Analysis of Journal Bearing with Partial Texture Lubricated Using Micropolar and Power-Law Fluids*, Springer: Cham, 2020, pp. 211–225.

[21] A. S. Lodge, *Elastic Liquids*, Academic Press: London and New York, 1964.

[22] R. C. Rosenberg, "A method for determining the influence of multigrad oils on journal bearing performance", *SAE Trans.* **82** (1973), pp. 1533–1545. Online at http://www.jstor.org/stable/44717562.

[23] V. K. Stokes, "Couple stresses in fluids", *Phys. Fluids* **9** (1966), no. 9, pp. 1709–1715.

[24] T. Ariman, M. A. Turk and N. D. Sylvester, "Micro continuum fluid mechanics-A review", *Int. J. Eng. Sci.* **11** (1973), no. 8, pp. 905–930.

[25] T. Ariman, M. A. Turk and N. D. Sylvester, "Applications of micro continuum fluid mechanics", *Int. J. Eng. Sci.* **12** (1974), no. 4, pp. 273–293.

[26] U. Mokhiamer, W. Crosby and H. El-Gamal, "A study of a journal bearing lubricated by fluids with couple stress considering the elasticity of the liner", *Wear* **224** (1999), no. 2, pp. 194–201.

[27] J. Lin, "Linear stability analysis of rotor-bearing system: couple stress fluid model", *Comput. Struct.* **79** (2001), no. 8, pp. 801–809.

[28] N. B. Naduvinamani, P. S. Hiremath and G. Gurubasavaraj, "Surface roughness effects in a short porous journal bearing with a couple stress fluid", *Fluid Dyn. Res.* **31** (2002), no. 5–6, pp. 333–354.

[29] A. Kabouya, M. Lahmar and B. S. Benyebka, "Analysis of misaligned plain journal bearings lubricated with couple-stress fluids", *Mech. Indust.* **8** (2007), pp. 577–595. French.

[30] B. A. Abass and M. A. Mahdi, "Effect of micro protrusions on the performance of elliptical journal bearings operating with couple stress lubricant", *Diagnostyka* **22** (2021), no. 2, pp. 97–104.

[31] X. Wang, K. Zhu and S. Wen, "Thermohydrodynamic analysis of journal bearings lubricated with couple stress fluids", *Tribol. Int.* **34** (2001), no. 5, pp. 335–343.

[32] S. Kango and R. K. Sharma, "Studies on the influence of surface texture on the performance of hydrodynamic journal bearing using power law model", *Int. J. Surf. Sci. Eng.* **4** (2010), no. 4/5/6, pp. 505–524.

[33] B. J. Hamrock, *Fundamental of Fluid Film Lubrication*, NASA reference publication 1255, McGraw-Hill: New York, 1994. Online at https://ntrs.nasa.gov/api/citations/19910021217/downloads/19910021217.pdf.

[34] D. G. Christopherson, "A new mathematical method for the solution of film lubrication problems", *Proc. Inst. Mech. Eng.* **146** (1941), no. 1, pp. 126–135.

[35] V. N. Constantinescu, A. L. Nica, M. D. Pascovici, G. Ceptureanu and S. Nedelcu, *Sliding Bearings*, Allerton Press Inc.: New York, 1985.